https://doi.org/10.5194/egusphere-2026-2672
Preprint. Discussion started: 23 June 2026

Propagation of Instrumental Self-Noise Through Causal Response Correction: Implications for Seismic-Network Detectability and Completeness

Antonino D'Alessandro
Istituto Nazionale di Geofisica e Vulcanologia, Osservatorio Nazionale, Rome, Italy
antonino.dalessandro@ingv.it
https://orcid.org/0000-0002-0074-3125

Abstract

Seismic detectability is commonly interpreted as a consequence of network geometry, station density, and environmental noise. However, instrumental self-noise and causal instrument correction can substantially modify the effective station noise floor and therefore influence earthquake detectability and completeness magnitude. Despite their importance in instrumental seismology, these effects are rarely incorporated explicitly into network-scale detectability analyses. This study develops a unified theoretical and computational framework linking instrumental response, causal response correction, ground-referred self-noise, environmental seismic noise, station-level signal-to-noise ratio, probabilistic detection, and network-scale completeness magnitude. The framework propagates instrumental self-noise through the inverse instrumental response into corrected ground-motion units and integrates this contribution into a probabilistic detectability formalism. Global broadband station geometries derived from publicly available FDSN metadata are combined with physically informed environmental-noise fields and parameterized instrumental self-noise models to investigate large-scale detectability behavior. The results demonstrate that seismic detectability emerges from the coupled interaction among network geometry, environmental noise, and propagated instrumental self-noise. Three principal operational regimes arise naturally from the framework: geometry-limited, ambient-noise-limited, and self-noise-limited detectability conditions. Sparse networks are dominated primarily by geometric effects, whereas densely instrumented low-noise networks become increasingly sensitive to instrumental self-noise after causal response correction. The results further show that the marginal detectability

https://doi.org/10.5194/egusphere-2026-2672
Preprint. Discussion started: 23 June 2026

gain associated with network densification progressively decreases as station density increases, while the relative importance of instrumental quality correspondingly grows. The framework additionally demonstrates that instrumental self-noise may be substantially amplified near the limits of the instrumental passband after response correction, producing detectability degradation even when raw instrumental-noise levels appear comparatively small. Consequently, seismic-network performance cannot be interpreted exclusively as a geometrical property, but instead reflects a multiscale interaction among instrument physics, environmental conditions, and network organization. The proposed methodology provides a computationally reproducible and physically interpretable basis for analyzing detectability limits and regime-dependent network optimization in modern seismic monitoring systems, including dense broadband arrays and emerging low-cost MEMS-based networks. The proposed methodology is intended primarily as a physically interpretable framework for investigating first-order detectability controls and regime-dependent network optimization rather than as an operational estimator of real-world global completeness magnitude.

1. Introduction

Modern seismic monitoring systems are increasingly evaluated not only in terms of instrumental sensitivity, bandwidth, dynamic range, or installation quality, but also through their effective capability to detect, identify, and characterize seismic signals across a broad range of magnitudes, distances, site conditions, and network geometries. In operational seismology, this capability is commonly summarized through the concept of detectability, namely the probability that an earthquake signal exceeds the effective observational threshold of a seismic station or network and can therefore be reliably detected, associated, and processed. Detectability directly controls the magnitude of completeness M_c, which in turn governs the reliability of earthquake catalogues, seismicity-rate estimates, b-value calculations, earthquake forecasting models, and seismic-hazard assessments.

Traditionally, detectability and catalogue completeness have been interpreted primarily as consequences of network geometry, station spacing, azimuthal coverage, environmental noise, and phase-picking performance. Simulation-based approaches have been developed to assess the location capability and magnitude thresholds of real seismic networks, including the Seismic Network Evaluation through Simulation (SNES) framework

https://doi.org/10.5194/egusphere-2026-2672
Preprint. Discussion started: 23 June 2026

applied to national and regional monitoring systems (D'Alessandro et al., 2011; D'Alessandro and Ruppert, 2012; D'Alessandro and Stickney, 2012). These studies demonstrated that network performance is spatially heterogeneous and strongly dependent on station geometry, phase availability, and regional coverage. Similar analyses were later extended to the evolution and strengthening of regional seismic networks (D'Alessandro et al., 2013a). However, these approaches primarily focused on geometrical and statistical aspects of network performance rather than on the propagation of instrumental noise through response correction.

In parallel, ambient seismic-noise characterization has become a standard tool for evaluating station quality and monitoring performance. The New Low Noise Model (NLNM) and New High Noise Model (NHNM) introduced by Peterson (1993) remain foundational references for broadband seismic-noise assessment, while probabilistic power spectral density approaches have enabled quantitative characterization of the temporal and spatial variability of seismic background noise (McNamara and Buland, 2004). More recently, spatial analyses of seismic-noise variability have shown that ambient-noise levels can significantly influence network detectability and completeness magnitude. Detailed PSD/PDF analyses performed on the Italian Seismic Network further demonstrated the strong spatial and temporal variability of background seismic noise and its direct implications for seismic-network detectability and completeness magnitude (D'Alessandro et al., 2021). In particular, Catania et al. (2025) demonstrated a strong spatial correspondence between background seismic-noise levels and completeness-magnitude variability within the Italian seismic network, emphasizing that detectability cannot be interpreted exclusively as a geometrical property of the network. Similarly, the development of quasi-real-time seismic-noise monitoring systems, such as SEISMONOISY (Ruzza et al., 2024), highlights the increasing importance of dynamic noise-field characterization for operational seismic-network assessment and optimization.

Instrumental self-noise has long been recognized as a limiting factor in broadband seismology and sensor characterization. Three-channel correlation techniques provide rigorous estimates of the intrinsic self-noise of digitizers and seismic sensors (Sleeman et al., 2006), and subsequent studies demonstrated that instrumental self-noise depends strongly on sensor type, frequency band, installation conditions, and sensor orientation (Gerner and Bokelmann, 2013; Wang et al., 2023). Recent analyses comparing multiple seismometer classes further confirmed that no single instrument minimizes self-noise across the entire seismic frequency spectrum

https://doi.org/10.5194/egusphere-2026-2672
Preprint. Discussion started: 23 June 2026

(Wang et al., 2023). Consequently, detectability depends not only on environmental noise and source amplitude, but also on the interaction between instrumental response and intrinsic sensor noise.

These issues become even more relevant in the context of emerging dense and low-cost seismic networks. MEMS accelerometers and compact low-cost sensors have enabled new monitoring strategies for urban seismology, structural health monitoring, rapid post-earthquake assessment, and dense local earthquake detection. D'Alessandro and D'Anna (2013) evaluated the suitability of low-cost MEMS accelerometers for strong-motion seismology, while D'Alessandro et al. (2014) proposed an urban MEMS-based seismic network for rapid post-earthquake disaster assessment. D'Alessandro et al. (2017) subsequently characterized MEMS accelerometer self-noise using power spectral density and Allan variance analysis, demonstrating that self-noise characterization is essential before low-cost sensors can be reliably integrated into seismic monitoring systems. More recent studies and reviews further highlighted the rapid evolution of urban and distributed seismic networks based on heterogeneous low-cost instrumentation (Anthony et al., 2019; Vitale et al., 2022; Scudero et al., 2023).

These developments are particularly important because dense low-cost networks inherently modify the balance between geometry-driven and instrumentation-driven detectability limitations. In sparse networks, detectability is primarily controlled by inter-station spacing and azimuthal coverage. However, as network density increases, instrumental self-noise progressively becomes a non-negligible contribution to the effective detection threshold, especially after instrument-response correction into ground-motion units. Under these conditions, detectability can no longer be interpreted solely as a consequence of network geometry or ambient noise.

Despite these advances, a conceptual gap still exists between instrumental self-noise characterization and network-scale detectability analysis. Existing studies commonly treat self-noise as a station-level instrumental property, whereas detectability and M_c are usually considered network-level quantities controlled by geometry and environmental noise. However, seismic waveforms are not interpreted directly in recorded digital units. Instead, instrumental response removal or causal correction is applied to estimate the underlying ground motion. This operation maps instrumental self-noise into ground-motion units through the inverse transfer function of the sensor–digitizer system, potentially amplifying specific frequency bands near the instrumental

https://doi.org/10.5194/egusphere-2026-2672
Preprint. Discussion started: 23 June 2026

limits. As a consequence, the effective station noise floor depends simultaneously on environmental noise, instrumental self-noise, and the spectral properties of the response correction.

The central conceptual contribution of this work is the explicit propagation of instrumental self-noise through causal response correction into probabilistic network-detectability metrics, thereby establishing a direct physical link between instrument-response physics and large-scale seismic monitoring performance.

The present study develops a unified theoretical and computational framework that links instrument physics, causal response correction, ground-referred self-noise, station-level signal-to-noise ratio, probabilistic station detection, and network-scale detectability into a single physically consistent formalism. The central hypothesis of this work is that seismic detectability is an emergent multiscale property resulting from the coupled interaction among: (i) source amplitude and spectral content, (ii) propagation effects, (iii) environmental noise, (iv) instrumental self-noise, (v) causal instrument correction, and (vi) network aggregation geometry.

Within this framework, instrumental self-noise is propagated into corrected ground-motion units through the inverse instrumental response, allowing the definition of an effective station noise floor that combines environmental and instrumental contributions. This effective noise model is then integrated into a probabilistic station-detection formalism and subsequently aggregated into network-scale detectability metrics and spatial completeness fields.

The manuscript further introduces the concept of detectability regimes. Depending on network density, ambient noise, and effective self-noise, a monitoring system may operate in a geometry-limited regime, an ambient-noise-limited regime, or a self-noise-limited regime. These regimes imply fundamentally different optimization strategies for seismic-network design. In sparse networks, densification may provide the dominant gain in detectability. In dense networks, reducing instrumental self-noise may become more effective than adding further stations. Intermediate configurations instead require joint optimization of station geometry and sensor quality.

The objectives of this work are therefore fourfold: (1) to formalize the propagation of instrumental self-noise through causal instrument correction; (2) to define an effective station noise floor combining environmental and ground-referred instrumental noise; (3) to quantify the effect of this effective noise on station-level and network-level detectability; and (4) to establish a regime-aware framework for seismic-network optimization linking instrument physics to network performance.

https://doi.org/10.5194/egusphere-2026-2672
Preprint. Discussion started: 23 June 2026

Figure 1 summarizes the conceptual architecture of the proposed framework, illustrating the physical chain connecting ground motion, instrumental response, self-noise propagation, station-level signal-to-noise ratio, probabilistic detection, and network-scale detectability metrics. The purpose of the present study is therefore not to provide an operational estimate of global earthquake detectability or catalogue completeness, but rather to establish a physically consistent and computationally reproducible framework capable of isolating and quantifying the first-order interactions between causal instrument correction, propagated instrumental self-noise, environmental seismic noise, and network geometry. Within this perspective, the proposed methodology should be interpreted primarily as a regime-oriented and physically interpretable detectability framework designed to investigate how instrumental and geometrical limitations jointly control seismic monitoring performance across different network configurations.

2. Theoretical Framework

The detectability of seismic signals by a monitoring network is ultimately controlled by the coupled interaction among source radiation, wave propagation, environmental noise, instrumental response, and network geometry. In standard seismic processing, recorded waveforms are transformed from instrumental digital counts into estimates of physical ground motion through response removal or causal instrument correction. This operation fundamentally modifies the spectral structure of both signal and noise, implying that detectability must be formulated in corrected ground-motion units rather than in raw instrumental counts. The framework developed in this work explicitly propagates instrumental self-noise through causal response correction and integrates it into a probabilistic network-detectability formalism. Figure 2 illustrates the spectral propagation of environmental and instrumental noise contributions into the effective station noise floor.

Let $g(t)$ denote the true ground-motion signal and $h_i(t)$ the causal impulse response of the i-th seismic station, including sensor, digitizer, and acquisition chain. The recorded waveform $d_i(t)$ can be written as

$$d_i(t) = h_i(t) * g(t) + n_i^{\mathrm{env}}(t) + n_i^{\mathrm{self}}(t), \qquad (1)$$

https://doi.org/10.5194/egusphere-2026-2672
Preprint. Discussion started: 23 June 2026

where $n_i^{\mathrm{env}}(t)$ represents the environmental noise contribution, $n_i^{\mathrm{self}}(t)$ is the intrinsic instrumental self-noise, and $*$denotes convolution.

In the frequency domain, Eq. (1) becomes

$$D_i(\omega) = H_i(\omega)G(\omega) + N_i^{\mathrm{env}}(\omega) + N_i^{\mathrm{self}}(\omega). \qquad (2)$$

To estimate the underlying ground motion, the instrumental response is removed through inverse filtering. In practical applications, strictly acausal deconvolution is generally avoided because it may amplify unstable spectral components and violate real-time processing constraints. The corrected signal is therefore obtained through stabilized causal correction:

$$\hat{G}_i(\omega) = \frac{D_i(\omega)}{H_i(\omega)} W_i(\omega), \qquad (3)$$

where $W_i(\omega)$ is a stabilization operator accounting for regularization, tapering, and causal filtering constraints. Such stabilization procedures are necessary to avoid numerical instabilities and non-physical amplification near zeros of the instrumental response (Scherbaum, 2001; Wielandt, 2002).

Substituting Eq. (2) into Eq. (3) yields

$$\hat{G}_i(\omega) = G(\omega)W_i(\omega) + \frac{N_i^{\mathrm{env}}(\omega)}{H_i(\omega)} W_i(\omega) + \frac{N_i^{\mathrm{self}}(\omega)}{H_i(\omega)} W_i(\omega). \qquad (4)$$

Equation (4) highlights a key physical aspect of the problem: instrumental self-noise is transformed into corrected ground-motion units through the inverse response of the instrument. Consequently, the detectability threshold depends not only on environmental noise and source amplitude, but also on the spectral amplification induced by response correction.

The power spectral density (PSD) of the ground-referred instrumental self-noise is defined as

https://doi.org/10.5194/egusphere-2026-2672
Preprint. Discussion started: 23 June 2026

$$S_{n,i}^{\mathrm{self,gr}}(\omega) = \frac{S_{n,i}^{\mathrm{self}}(\omega)}{|\, H_i(\omega)\,|^2}. \qquad (5)$$

Here, $S_{n,i}^{\mathrm{self}}(\omega)$ denotes the intrinsic instrumental self-noise PSD and $H_i(\omega)$ is the complex transfer function of the instrument. Equivalent formulations are commonly used in instrumental self-noise characterization and seismic sensor intercomparison studies (Sleeman et al., 2006; Ringler and Hutt, 2010). Equation (5) further shows that response correction may significantly amplify instrumental noise near the limits of the instrumental passband, especially at long periods and high frequencies where $|\, H_i(\omega)\,|$ becomes small. This effect is illustrated conceptually in Figure 2.

The total effective station noise floor is modeled as the sum of environmental and ground-referred instrumental noise:

$$S_{n,i}^{\mathrm{eff}}(\omega) = S_{n,i}^{\mathrm{env}}(\omega) + S_{n,i}^{\mathrm{self,gr}}(\omega). \qquad (6)$$

This formulation assumes statistical independence between environmental and instrumental noise sources. Although this assumption may not hold strictly under all installation conditions, it provides a first-order approximation suitable for network-scale detectability modeling. The formulation is conceptually consistent with probabilistic PSD/PDF approaches commonly used in broadband seismic-noise characterization (Peterson, 1993; McNamara and Buland, 2004). Figure 3 illustrates the transition from station-level detectability kernels to network-scale completeness and spatial detectability fields obtained through probabilistic aggregation of multiple stations.

Let $S_s(M, r, \omega)$ denote the source spectrum associated with an earthquake of magnitude Mat hypocentral distance r. The station-level signal-to-noise ratio is defined as

$$\mathrm{SNR}_i(M, r, \omega) = \frac{S_s(M, r, \omega)}{S_{n,i}^{\mathrm{eff}}(\omega)}. \qquad (7)$$

https://doi.org/10.5194/egusphere-2026-2672
Preprint. Discussion started: 23 June 2026

The source spectrum may include attenuation, geometrical spreading, radiation-pattern effects, and site amplification terms. In this work, the framework is intentionally formulated in a general form independent of a specific attenuation law in order to preserve broad applicability.

For practical detectability estimates, a band-integrated SNR is considered:

$$\mathrm{SNR}_i^{\mathrm{band}}(M,r) = \int_{\omega_1}^{\omega_2} W_b(\omega)\, \mathrm{SNR}_i(M,r,\omega)\, d\omega, \qquad (8)$$

where $W_b(\omega)$ is a frequency-weighting function defining the target detection band. Band-integrated SNR metrics are widely used in seismic-station performance evaluation and automatic event-detection systems (Trnkoczy, 2012). Figure 4 illustrates the propagation of effective station noise into frequency-dependent SNR degradation and station-level detectability.

Detection is modeled probabilistically rather than deterministically. Let $P_i(M,x)$ denote the probability that the i-th station detects an earthquake of magnitude Moccurring at spatial position x. Following a generalized logistic formulation,

$$P_i(M,x) = \frac{1}{1+\exp\left[-\alpha_i\left(\mathrm{SNR}_i^{\mathrm{band}}(M,x)-\theta_i\right)\right]}, \qquad (9)$$

where θ_i is the effective detection threshold and α_i controls the steepness of the transition between non-detection and detection. This probabilistic formulation accounts for the gradual transition between detectable and non-detectable conditions resulting from noise variability and waveform uncertainty. Taken together, Eqs. (1)–(9) define a unified detectability formalism in which instrumental self-noise becomes dynamically coupled to seismic-network performance through causal response correction and probabilistic network aggregation.

The network-level probability of detection is defined as the complement of the probability that all stations fail to detect the event:

https://doi.org/10.5194/egusphere-2026-2672
Preprint. Discussion started: 23 June 2026

$$P_{\text{detect}}(M,x) = 1 - \prod_{i=1}^{N}[1 - P_i(M,x)]. \qquad (10)$$

Equation (10) represents a simplified independence model in which station detections are treated as statistically independent conditional on the event parameters. Although this assumption neglects correlated noise, telemetry losses, and phase-association complexity, it provides a tractable first-order approximation for large-scale detectability analysis. Probabilistic formulations of seismic-network detection capability have long been used in seismic monitoring and network optimization studies (Ringdal, 1975; Kværna and Ringdal, 1986).

The completeness magnitude $M_c(x)$ is then defined as the minimum magnitude satisfying

$$P_{\text{detect}}(M_c,x) \geq P_0, \qquad (11)$$

where P_0 is a target detection probability, typically chosen between 0.9 and 0.95. Figure 5 illustrates the resulting spatial detectability fields and the emergence of completeness patterns jointly controlled by geometry and effective station noise.

The framework naturally predicts the existence of distinct detectability regimes depending on the relative importance of geometry, environmental noise, and instrumental self-noise. The geometry-limited regime is characterized by

$$\frac{\partial M_c}{\partial \log_{10} N} \gg \frac{\partial M_c}{\partial S_{\text{self}}}, \qquad (12)$$

where detectability is controlled primarily by station density and spatial coverage.

The self-noise-limited regime is characterized by

$$\frac{\partial M_c}{\partial S_{\text{self}}} \gg \frac{\partial M_c}{\partial \log_{10} N}, \qquad (13)$$

where instrumental self-noise dominates the effective detection threshold.

https://doi.org/10.5194/egusphere-2026-2672
Preprint. Discussion started: 23 June 2026

The ambient-noise-limited regime is characterized by

$$S_n^{\mathrm{env}}(\omega) \gg S_n^{\mathrm{self,gr}}(\omega), \qquad (14)$$

where environmental noise overwhelms the instrumental contribution.

These regimes define distinct optimization strategies for seismic-network design and are investigated quantitatively in Figures 6 and 7.

The complete framework developed in this work links instrumental response physics, causal correction, ground-referred self-noise, station-level SNR, probabilistic detection, network aggregation, and spatial completeness magnitude into a unified end-to-end detectability formalism. Figure 8 summarizes this conceptual architecture and illustrates how network performance emerges from the coupled interaction between instrumental properties, environmental noise, and network geometry.

3. Data

The framework developed in this study is intentionally designed to remain general and transferable across different classes of seismic monitoring systems. The adopted datasets are intentionally designed to support a physically interpretable and computationally reproducible exploration of first-order detectability controls rather than an operational reconstruction of real-world global catalogue completeness. Consequently, the present framework should be interpreted as a surrogate but physically grounded representation of the coupled interactions among network geometry, environmental noise, instrumental self-noise, and causal response correction. Figure 3 summarizes the transition from station-level detectability kernels to network-scale completeness and spatial detectability fields, while Figures 5–7 illustrate the resulting detectability patterns and regime classifications.

The station geometry used throughout this work is derived from publicly accessible metadata distributed through international FDSN web services, including EarthScope/IRIS and EIDA infrastructures (IRIS DMC, 2014; EIDA Consortium, 2023). Only broadband seismic stations equipped with high-gain channels (BH?,

https://doi.org/10.5194/egusphere-2026-2672
Preprint. Discussion started: 23 June 2026

HH?, LH?) were considered in order to maintain consistency with the broadband detectability framework investigated here. The retrieved station metadata include latitude, longitude, network code, station code, and operational status. After merging and removing duplicate entries, the resulting global inventory contains several thousand broadband seismic stations with heterogeneous spatial coverage representative of current large-scale monitoring systems.

The adopted station distribution exhibits dense coverage across North America, Europe, Japan, and selected tectonically active regions, whereas large portions of oceanic domains, polar regions, continental interiors, and developing regions remain sparsely instrumented. This spatial heterogeneity is a fundamental component of the present analysis because it naturally generates geometry-controlled variations in detectability and completeness magnitude. The resulting network geometry therefore provides a realistic first-order approximation of the present-day global broadband monitoring infrastructure, despite unavoidable temporal variations in station availability, instrumentation, and operational status.

The present framework does not explicitly simulate waveform propagation through three-dimensional Earth structure. Instead, detectability is modeled through simplified geometry-dependent attenuation kernels designed to isolate the first-order interaction between source amplitude, source-to-station distance, and effective station noise. This choice intentionally prioritizes physical interpretability, numerical stability, and computational reproducibility over regional propagation realism. Consequently, the resulting detectability fields should not be interpreted as operational estimates of absolute completeness magnitude, but rather as internally consistent representations of relative detectability variability.

Environmental seismic noise is represented through synthetic but physically informed global noise fields constructed to mimic the large-scale spatial variability observed in broadband seismic-noise studies (Peterson, 1993; McNamara and Buland, 2004). The adopted environmental-noise model includes broad continental-scale gradients and regionalized perturbations intended to approximate the contrast between low-noise continental interiors, moderate-noise tectonically active regions, and high-noise coastal or urbanized environments. The adopted representation therefore preserves realistic large-scale spatial structure without attempting to reproduce site-specific noise spectra or temporal nonstationarity.

The environmental noise level associated with the i-th station is represented through the PSD field $S_{n,i}^{\mathrm{env}}(\omega)$, while instrumental self-noise is introduced through a family of parameterized spectral models representing

https://doi.org/10.5194/egusphere-2026-2672
Preprint. Discussion started: 23 June 2026

different instrumental quality classes. Rather than assigning manufacturer-specific self-noise curves to individual stations, the analysis adopts representative self-noise scenarios spanning low-noise broadband instruments, intermediate-quality sensors, and higher-noise compact or low-cost instrumentation. This approach allows systematic exploration of the transition between geometry-limited and self-noise-limited detectability regimes.

The self-noise representation is intentionally simplified and does not attempt to reproduce the detailed spectral behavior of individual sensors. In particular, the present study neglects possible variations associated with installation quality, vault conditions, digitizer characteristics, sensor orientation, aging effects, calibration uncertainties, or site-specific coupling effects. Nevertheless, the adopted parameterization preserves the first-order physical mechanism through which causal response correction propagates instrumental noise into corrected ground-motion units.

To evaluate network-scale detectability, the Earth's surface is discretized onto a regular latitude–longitude grid. For each grid node, the source-to-station distance is computed relative to all available stations, allowing construction of station-level detectability kernels and subsequent probabilistic aggregation into network detection probability $P_{\mathrm{detect}}(M, x)$. Spatial smoothing is then applied to reduce discretization artifacts and emphasize large-scale detectability patterns rather than grid-dependent local fluctuations. Figures 5 and 6 show the resulting global detectability fields and regime classifications.

The detectability calculations are intentionally performed within a generic frequency-domain framework rather than for a specific earthquake source model. The source spectrum $S_s(M, r, \omega)$ is therefore treated parametrically, allowing the framework to remain independent of any single attenuation relation, stress-drop model, or regional propagation law. This choice reflects the primary objective of the manuscript, namely the investigation of how instrumental self-noise and network geometry jointly control detectability after causal instrument correction.

Several assumptions and limitations must therefore be emphasized. First, the present framework does not incorporate realistic phase picking, event association, waveform correlation, or machine-learning-based detection algorithms. Second, station detections are treated as conditionally independent in the probabilistic aggregation model. Third, the environmental-noise field is synthetic and spatially smoothed rather than derived directly from continuous waveform archives. Fourth, the source model neglects source complexity, focal

https://doi.org/10.5194/egusphere-2026-2672
Preprint. Discussion started: 23 June 2026

mechanism variability, frequency-dependent scattering, and three-dimensional propagation effects. Finally, the detectability fields presented in this work should be interpreted as physically informed sensitivity maps rather than operational completeness estimates.

Despite these limitations, the adopted dataset configuration provides a robust and reproducible framework for isolating the first-order coupling among causal instrument correction, ground-referred self-noise, network geometry, and seismic detectability. The resulting framework is therefore particularly suitable for investigating regime-dependent network optimization strategies and the transition between geometry-driven and instrumentation-driven detectability limits.

4. Methods

The methodological framework developed in this study is designed to quantify how instrumental self-noise, environmental noise, and network geometry jointly control seismic detectability after causal instrument correction. The workflow combines physically motivated station-level signal modeling with probabilistic network aggregation, allowing the construction of spatial detectability fields, completeness-magnitude maps, and regime-classification diagnostics. The complete workflow is summarized conceptually in Figure 8, while Figures 3–7 illustrate the successive stages of the computational framework.

The first step of the methodology consists of constructing an effective station noise model in corrected ground-motion units. For each station i, the environmental-noise PSD $S_{n,i}^{\mathrm{env}}(\omega)$ is combined with the ground-referred instrumental self-noise $S_{n,i}^{\mathrm{self,gr}}(\omega)$ defined in Eq. (5). The resulting effective station noise floor is therefore

$$S_{n,i}^{\mathrm{eff}}(\omega) = S_{n,i}^{\mathrm{env}}(\omega) + S_{n,i}^{\mathrm{self,gr}}(\omega). \qquad (15)$$

The effective noise field is evaluated over a broad frequency range representative of standard broadband seismic observations. The adopted spectral representation is intentionally simplified and is not intended to reproduce instrument-specific transfer functions in detail. Instead, the objective is to isolate the first-order contribution of response-corrected self-noise to detectability degradation. The adopted PSD-based

https://doi.org/10.5194/egusphere-2026-2672
Preprint. Discussion started: 23 June 2026

representation is conceptually consistent with probabilistic seismic-noise characterization methods widely used in broadband station monitoring (McNamara and Buland, 2004).

The source spectrum associated with an earthquake of magnitude Mat hypocentral distance $r$is represented through a generalized attenuation-based formulation:

$$S_s(M,r,\omega) = A(M,\omega)\, G(r)\, Q(r,\omega)\, R(\omega), \qquad (16)$$

where $A(M,\omega)$ represents source scaling, $G(r)$ accounts for geometrical spreading, $Q(r,\omega)$ represents attenuation effects, and $R(\omega)$ includes site and radiation-pattern contributions. The present framework intentionally avoids adopting a region-specific attenuation law in order to preserve generality and computational reproducibility.

For each station and grid node, the frequency-dependent signal-to-noise ratio is computed according to Eq. (7). A band-integrated station-level SNR is then evaluated using

$$\mathrm{SNR}_i^{\mathrm{band}}(M,r) = \int_{\omega_1}^{\omega_2} W_b(\omega)\, \frac{S_s(M,r,\omega)}{S_{n,i}^{\mathrm{eff}}(\omega)}\, d\omega, \qquad (17)$$

where $W_b(\omega)$ defines the frequency weighting within the target detection band. The adopted weighting function is smooth and broadband in order to avoid introducing artificial detectability discontinuities associated with narrow-band amplification. Band-integrated SNR metrics are widely used in seismic-station performance evaluation and automatic event-detection systems (Trnkoczy, 2012). Figure 4 illustrates the propagation of effective station noise into frequency-dependent SNR degradation and station-level detectability.

Detection is modeled probabilistically rather than deterministically. Let $P_i(M,x)$ denote the probability that the i-th station detects an earthquake of magnitude Moccurring at spatial position x. Following a generalized logistic formulation,

https://doi.org/10.5194/egusphere-2026-2672
Preprint. Discussion started: 23 June 2026

$$P_i(M,x) = \frac{1}{1+\exp\left[-\alpha_i\left(\mathrm{SNR}_i^{\mathrm{band}}(M,x)-\theta_i\right)\right]}, \qquad (18)$$

where θ_i represents the effective station detection threshold and α_i controls the steepness of the detectability transition. This probabilistic representation accounts for the fact that detection capability does not exhibit a sharp binary threshold, but rather transitions gradually as a function of signal amplitude and noise conditions. Similar probabilistic formulations are commonly adopted in seismic-network performance and automatic-detection studies (Ringdal, 1975; Allen, 1978; Withers et al., 1996).

The spatial detectability kernel associated with each station is computed by evaluating Eq. (18) over the full latitude–longitude grid. Figure 3 illustrates the resulting station-level kernels and their aggregation into network-scale detectability fields. The kernel approach allows efficient evaluation of large-scale detectability variability while preserving explicit dependence on station geometry and effective station noise. Kernel-based representations of seismic-network performance are conceptually related to simulation-based network evaluation frameworks such as SNES (D'Alessandro et al., 2011; D'Alessandro and Ruppert, 2012).

Network-level detectability is then computed using the probabilistic aggregation model introduced in Eq. (10):

$$P_{\mathrm{detect}}(M,x) = 1 - \prod_{i=1}^{N}[1-P_i(M,x)]. \qquad (19)$$

This formulation assumes conditional independence among station detections. Although this assumption neglects correlated environmental noise, telemetry failures, and event-association complexity, it provides a computationally tractable first-order approximation for large-scale detectability analysis. Probabilistic formulations of seismic-network detection capability have long been used in seismic monitoring and network optimization studies (Ringdal, 1975; Kværna and Ringdal, 1986).

The completeness magnitude $M_c(x)$ is estimated by solving

$$P_{\mathrm{detect}}(M_c,x) = P_0, \qquad (20)$$

https://doi.org/10.5194/egusphere-2026-2672
Preprint. Discussion started: 23 June 2026

where P_0 is the target detection probability threshold. In this work, P_0 is fixed at 0.95 unless otherwise stated. Figure 5 illustrates the resulting spatial detectability maps and completeness fields.

To reduce discretization artifacts associated with the finite spatial grid and heterogeneous station spacing, spatial smoothing is applied to the detectability fields using isotropic Gaussian filtering. The smoothing scale is intentionally chosen to suppress grid-dependent fluctuations while preserving first-order continental-scale detectability gradients. Spatial smoothing approaches are commonly used in completeness and seismic-network capability studies to stabilize large-scale detectability patterns and suppress artificial discretization effects (Woessner and Wiemer, 2005). No attempt is made to infer local operational completeness values at subregional scales.

The framework additionally evaluates the relative sensitivity of detectability to network geometry and instrumental self-noise. The geometry sensitivity is quantified through

$$\Gamma_N = -\frac{\partial M_c}{\partial \log_{10} N}, \qquad (21)$$

while the self-noise sensitivity is quantified as

$$\Gamma_{\text{self}} = \frac{\partial M_c}{\partial S_{\text{self}}}, \qquad (22)$$

These two quantities are used to classify the dominant detectability regime at each grid node. Figure 6 shows the resulting regime-classification maps, while Figure 7 illustrates the trade-off between geometry-driven and self-noise-driven detectability limitations.

The regime-classification framework distinguishes among geometry-limited, self-noise-limited, and ambient-noise-limited conditions according to the relative magnitude of Γ_N, Γ_{self}, and the environmental-noise contribution. This classification provides a physically interpretable representation of how detectability controls change across different network configurations and instrumental conditions.

Several methodological simplifications must nevertheless be emphasized. The framework does not include realistic phase picking, waveform correlation, template matching, machine-learning-based detectors, or event-

https://doi.org/10.5194/egusphere-2026-2672
Preprint. Discussion started: 23 June 2026

association algorithms. Source radiation is represented through simplified isotropic spectral scaling, while three-dimensional Earth structure and path-dependent scattering are neglected. Furthermore, the environmental-noise model is synthetic and temporally stationary. Consequently, the present methodology should be interpreted as a first-order physical framework for network detectability analysis rather than as an operational earthquake-detection simulator.

Despite these limitations, the adopted methodology provides a computationally reproducible and physically transparent framework for quantifying how causal instrument correction propagates instrumental self-noise into seismic detectability and completeness magnitude. The resulting approach is particularly suitable for investigating the transition between geometry-controlled and instrumentation-controlled monitoring regimes in modern seismic networks.

5. Results

The proposed framework reveals that seismic detectability emerges from the coupled interaction among network geometry, environmental noise, and instrumental self-noise after causal instrument correction. The resulting detectability patterns exhibit strong spatial variability and naturally organize into distinct operational regimes characterized by different dominant limiting factors. Figures 3–7 summarize the principal results obtained from the station-level detectability kernels, network aggregation framework, and regime-classification analysis.

Figure 3 illustrates the transition from individual station detectability kernels to network-scale completeness fields. The station-level kernels exhibit the expected radial attenuation structure around individual stations, with detectability decreasing progressively as source-to-station distance increases. However, the aggregated network response is highly heterogeneous at the global scale due to the strongly nonuniform spatial distribution of broadband seismic stations. Dense continental regions characterized by high station density exhibit extensive overlapping detectability kernels, producing elevated network detection probabilities and reduced completeness magnitude. In contrast, oceanic domains, polar regions, and sparsely instrumented continental interiors display fragmented detectability structures associated with limited network redundancy.

https://doi.org/10.5194/egusphere-2026-2672
Preprint. Discussion started: 23 June 2026

The resulting global completeness patterns shown in Figure 5 demonstrate that network geometry alone produces strong first-order spatial variability in detectability. Regions characterized by dense station coverage exhibit systematically lower $M_c$values, whereas sparsely instrumented regions require substantially larger event magnitudes to achieve the same network-level detection probability. Similar geometry-controlled completeness variations have previously been observed in simulation-based seismic-network performance analyses (D'Alessandro et al., 2011; D'Alessandro and Ruppert, 2012). These geometry-controlled gradients emerge naturally from the probabilistic aggregation framework and remain stable under moderate variations in smoothing scale and detection threshold.

The introduction of environmental noise significantly modifies the spatial detectability structure. Figure 4 shows that elevated environmental-noise levels reduce the effective station-level signal-to-noise ratio and broaden the transition between detectable and non-detectable conditions. This behavior is consistent with previous studies linking ambient seismic-noise levels to station performance and completeness variability (McNamara and Buland, 2004; Catania et al., 2025). The degradation of detectability is nonlinear because the logistic detection model amplifies the effect of small SNR perturbations near the effective detection threshold.

The impact of instrumental self-noise becomes evident after causal response correction. Figure 2 demonstrates that response correction propagates instrumental self-noise into corrected ground-motion units through the inverse instrumental transfer function. Such amplification effects are consistent with established instrumental self-noise analyses and sensor intercomparison studies (Sleeman et al., 2006; Ringler and Hutt, 2010). Although environmental noise remains the dominant contribution across most of the broadband frequency range, instrumental self-noise becomes increasingly important at long periods and in low-noise monitoring conditions. This effect is particularly pronounced for higher-noise instrumental classes and low-cost sensing configurations.

Figure 4 further demonstrates that the contribution of instrumental self-noise is strongly frequency dependent. In the low-frequency domain, response correction may substantially increase the effective station noise floor even when the intrinsic instrumental noise remains relatively small in raw instrumental units. Consequently, detectability degradation cannot be interpreted solely as a function of environmental noise amplitude, but must also account for the spectral behavior of the corrected instrumental response.

https://doi.org/10.5194/egusphere-2026-2672
Preprint. Discussion started: 23 June 2026

The global detectability fields shown in Figure 5 reveal that the interaction between environmental noise and instrumental self-noise produces spatially variable detectability degradation. In regions already characterized by sparse station geometry, self-noise amplification produces relatively modest additional effects because geometry remains the dominant limiting factor. In contrast, densely instrumented low-noise regions exhibit significantly greater sensitivity to instrumental self-noise because geometry-related limitations are already minimized. This result demonstrates that the relative importance of instrumental quality increases as network density improves. This geometry-to-self-noise transition represents one of the principal conceptual outcomes of the framework because it demonstrates that the dominant control on detectability evolves systematically as seismic networks approach increasingly dense monitoring configurations. This transition is particularly relevant for emerging dense and low-cost seismic networks, where instrumentation-related limitations may progressively dominate over purely geometrical constraints (Anthony et al., 2019; Scudero et al., 2023).

The regime-classification analysis shown in Figure 6 provides a quantitative representation of these transitions. Three principal detectability regimes emerge naturally from the framework. Comparable trade-offs between network geometry, environmental noise, and monitoring capability have been discussed in previous seismic-network optimization studies (Ringdal, 1975; D'Alessandro and Stickney, 2012). The geometry-limited regime dominates oceanic domains, remote continental interiors, and polar regions characterized by sparse station coverage. In these regions, detectability improvements are controlled primarily by increasing station density and reducing inter-station spacing. The ambient-noise-limited regime is concentrated in regions characterized by elevated environmental-noise levels, including coastal zones, tectonically active regions, and urbanized environments. In these areas, reductions in ambient noise or improvements in site conditions produce larger detectability gains than additional network densification.

The self-noise-limited regime appears primarily within dense low-noise networks where environmental noise and geometry-related limitations are already relatively weak. In these conditions, the effective detection threshold becomes increasingly sensitive to the spectral properties of the instrumental response and the propagated ground-referred self-noise. This transition is particularly important because it implies that further improvements in detectability may require reductions in instrumental self-noise rather than additional stations. Figure 7 quantifies the trade-off between geometry-driven and instrumentation-driven detectability improvements. The sensitivity analysis demonstrates that the relative gain associated with network

https://doi.org/10.5194/egusphere-2026-2672
Preprint. Discussion started: 23 June 2026

densification decreases progressively as station density increases. At low station density, detectability improvements are dominated by geometric effects because additional stations substantially increase spatial redundancy and reduce hypocentral distance to the nearest sensor. However, beyond a critical network density, the marginal detectability gain associated with additional stations becomes progressively smaller.

In contrast, the relative importance of instrumental self-noise increases systematically with network density. The sensitivity curves shown in Figure 7 indicate that low-noise instrumental configurations produce only limited improvements in sparse networks, but become increasingly effective within already dense monitoring systems. This nonlinear transition represents one of the principal results of the present study because it demonstrates that optimal network design strategies depend strongly on the operational detectability regime.

The framework additionally shows that detectability degradation associated with instrumental self-noise is strongly scale dependent. Small increases in self-noise may produce negligible effects under geometry-limited conditions while generating substantial detectability losses in low-noise dense networks. Consequently, the same instrumental improvement may have dramatically different operational value depending on the surrounding network configuration.

The global detectability fields remain qualitatively stable under moderate variations in smoothing scale, detection threshold P_0, and parameterized self-noise amplitude. Although the absolute completeness values vary as expected, the large-scale spatial organization of geometry-limited, ambient-noise-limited, and self-noise-limited regions remains robust. This stability indicates that the regime-classification framework reflects intrinsic properties of the coupled detectability system rather than numerical artifacts associated with a particular parameter choice.

Overall, the results demonstrate that seismic detectability cannot be interpreted exclusively as a geometrical property of seismic networks. Instead, detectability emerges from a multiscale interaction among station geometry, environmental noise, instrumental response, and propagated self-noise after causal correction. The resulting framework provides a physically interpretable basis for analyzing the transition between geometry-controlled and instrumentation-controlled monitoring regimes in modern seismic networks.

6. Discussion

https://doi.org/10.5194/egusphere-2026-2672
Preprint. Discussion started: 23 June 2026

The results presented in this study demonstrate that seismic detectability is not controlled exclusively by network geometry, but instead emerges from the coupled interaction among station distribution, environmental noise, instrumental response, and propagated self-noise after causal instrument correction. The proposed framework therefore extends traditional interpretations of network performance by explicitly linking instrument physics to large-scale detectability behavior.

Conventional seismic-network assessments have generally focused on geometrical quantities such as inter-station spacing, azimuthal coverage, phase availability, and travel-time residuals (Ringdal, 1975; D'Alessandro et al., 2011; D'Alessandro and Ruppert, 2012). Within this perspective, detectability is typically interpreted as a predominantly geometric property that improves monotonically with increasing station density. The present results only partially support this interpretation. While geometry clearly dominates detectability in sparse monitoring systems, the framework shows that the relative importance of instrumental self-noise progressively increases as network density improves and environmental noise decreases.

This transition constitutes one of the central conceptual results of the study. In geometry-limited conditions, detectability is controlled primarily by source-to-station distance and network redundancy. Under these conditions, the addition of new stations produces substantial reductions in completeness magnitude because it improves both spatial coverage and probabilistic aggregation efficiency. However, once network geometry reaches sufficiently high density, the marginal benefit associated with additional stations decreases significantly. At this stage, propagated instrumental self-noise becomes increasingly important because the effective station noise floor approaches the ambient-noise level.

This behavior has important implications for modern seismic-network design. Dense broadband arrays, urban monitoring systems, distributed MEMS deployments, and emerging low-cost seismic networks are increasingly characterized by high station density but heterogeneous instrumental quality (Anthony et al., 2019; Scudero et al., 2023). In these contexts, further densification alone may no longer provide optimal detectability gains. Instead, improvements in instrumental self-noise, response stability, vault conditions, or environmental-noise mitigation may become equally or more effective than adding additional stations.

More fundamentally, the present framework demonstrates that instrumental self-noise cannot be treated as an isolated sensor property once causal response correction is applied, because the corrected self-noise becomes an emergent component of the probabilistic detectability structure of the entire seismic network.

https://doi.org/10.5194/egusphere-2026-2672
Preprint. Discussion started: 23 June 2026

The results further emphasize the importance of causal response correction in detectability analysis. Instrumental self-noise is commonly characterized in raw instrumental units, where it may appear negligible relative to environmental noise across much of the broadband frequency range (Sleeman et al., 2006; Ringler and Hutt, 2010). However, the present framework shows that response correction can substantially amplify self-noise contributions near the limits of the instrumental passband, particularly at long periods and high frequencies. Consequently, the detectability impact of self-noise cannot be evaluated independently of the response-removal procedure.

This aspect is especially relevant for low-cost instrumentation and MEMS-based seismic networks. Although low-cost sensors may provide acceptable performance in strong-motion applications or dense urban deployments (D'Alessandro and D'Anna, 2013; D'Alessandro et al., 2014), their effective detectability after response correction depends critically on the spectral behavior of the corrected self-noise floor. The present framework therefore provides a physically consistent basis for evaluating the operational trade-offs between station density and instrumental quality in dense low-cost monitoring systems.

The regime-classification framework introduced in this work additionally provides a physically interpretable representation of how detectability controls vary spatially. The geometry-limited regime dominates sparsely instrumented regions, where additional stations remain the primary mechanism for improving completeness magnitude. In contrast, ambient-noise-limited regions are controlled predominantly by environmental conditions and site characteristics. Finally, self-noise-limited regimes emerge preferentially within dense low-noise networks where geometry-related limitations have already been minimized. This classification highlights that optimal network-design strategies are intrinsically regime dependent.

The framework also helps explain why improvements in detectability may saturate in mature broadband seismic networks. Once station spacing becomes sufficiently small, the effective detection threshold no longer decreases proportionally with network density because the station-level noise floor imposes a lower bound on usable signal amplitude. This saturation effect naturally emerges from the probabilistic aggregation model and may partially explain the diminishing returns often observed in highly developed monitoring infrastructures.

Importantly, the primary objective of the present study is not the operational prediction of absolute completeness magnitude at regional or global scales, but rather the development of a physically interpretable framework capable of identifying the dominant controls governing seismic detectability under different

https://doi.org/10.5194/egusphere-2026-2672
Preprint. Discussion started: 23 June 2026

monitoring configurations. From this perspective, the simplified surrogate representations adopted here are intentional because they allow isolation of the first-order coupling mechanisms linking instrumental response physics, propagated self-noise, environmental noise, and network geometry. Several limitations nevertheless constrain the interpretation of the present results. First, the environmental-noise field adopted in this study is synthetic and temporally stationary. Real seismic-noise environments exhibit strong seasonal, meteorological, anthropogenic, and diurnal variability that may substantially modify short-term detectability conditions (McNamara and Buland, 2004; Ruzza et al., 2024). These effects have been extensively documented through PSD/PDF analyses of the Italian broadband seismic network (D'Alessandro et al., 2021). Second, the framework does not explicitly include realistic phase picking, waveform correlation, machine-learning detectors, or event-association procedures. Modern AI-based detection systems may partially compensate for elevated noise levels through improved signal extraction and pattern recognition.

Third, the present analysis neglects three-dimensional Earth structure, path-dependent attenuation variability, anisotropic propagation, and scattering effects. The adopted attenuation formulation is intentionally simplified in order to isolate first-order interactions between geometry and instrumental noise. Consequently, the derived detectability fields should be interpreted as physically informed sensitivity patterns rather than operational estimates of catalogue completeness.

The assumption of conditional independence among station detections also represents an important simplification. In real seismic networks, environmental noise may exhibit spatial correlation, telemetry failures may affect multiple stations simultaneously, and phase-association procedures introduce additional nonlinear dependencies. Although the adopted aggregation framework provides a tractable first-order approximation, future extensions could incorporate correlated detection statistics and time-dependent network reliability.

Several additional developments appear particularly promising. The framework could be extended to include empirical PSD databases derived from continuous waveform archives, allowing direct integration of observed station-noise statistics into detectability calculations. Similarly, instrument-specific transfer functions and measured self-noise curves could replace the simplified parameterized instrumental classes adopted here. Another important extension would involve coupling the framework with realistic earthquake source populations and three-dimensional propagation simulations to generate operational detectability forecasts.

https://doi.org/10.5194/egusphere-2026-2672
Preprint. Discussion started: 23 June 2026

The methodology may also prove useful for evaluating future dense nodal arrays and distributed MEMS-based monitoring systems. In such networks, station density may become sufficiently large that geometry-related limitations are almost entirely suppressed, shifting detectability control toward instrumental stability and environmental noise. Under these conditions, the optimization problem changes fundamentally from "where should new stations be installed?" to "what level of instrumental quality is required to achieve further detectability gains?"

More broadly, the results highlight the need to reinterpret seismic-network performance as a multiscale emergent property linking instrument physics, environmental conditions, and spatial network organization. Detectability is therefore not solely a geometrical characteristic of monitoring systems, but rather the outcome of coupled interactions operating across multiple physical and observational scales.

The framework developed here provides a computationally reproducible and physically interpretable basis for investigating these interactions. By explicitly propagating instrumental self-noise through causal response correction into network-scale detectability metrics, the present study establishes a direct conceptual bridge between instrumental seismology and probabilistic seismic-network performance analysis.

7. Conclusions

This study developed a unified theoretical and computational framework linking causal instrument correction, instrumental self-noise, environmental seismic noise, and network geometry to seismic detectability and completeness magnitude. The proposed approach explicitly propagates instrumental self-noise into corrected ground-motion units through the inverse instrumental response and integrates this contribution into a probabilistic network-detectability formalism.

The results demonstrate that seismic detectability is not controlled exclusively by network geometry. Instead, detectability emerges from the coupled interaction among source amplitude, propagation effects, environmental noise, instrumental response, and probabilistic network aggregation. This interaction naturally generates strong spatial variability in completeness magnitude and produces distinct detectability regimes characterized by different dominant limiting factors.

https://doi.org/10.5194/egusphere-2026-2672
Preprint. Discussion started: 23 June 2026

The framework identifies three principal operational regimes. Geometry-limited conditions dominate sparse monitoring systems where detectability is controlled primarily by inter-station spacing and spatial coverage. Ambient-noise-limited conditions occur where elevated environmental noise suppresses station-level signal-to-noise ratios independently of network density. Self-noise-limited conditions emerge preferentially within dense low-noise networks, where geometry-related limitations are already minimized and the effective station noise floor becomes increasingly controlled by propagated instrumental self-noise.

One of the principal results of the study is the demonstration that the relative importance of instrumental quality increases systematically with network density. In sparse networks, additional stations produce the largest detectability improvements because geometric redundancy dominates network performance. However, as station density increases, the marginal benefit associated with further densification progressively decreases, while the contribution of instrumental self-noise becomes increasingly significant. This transition implies that optimal network-design strategies are intrinsically regime dependent.

The results additionally demonstrate that causal response correction plays a fundamental role in detectability analysis. Instrumental self-noise that appears negligible in raw instrumental units may become substantially amplified after response correction near the limits of the instrumental passband. Consequently, the detectability impact of instrumental noise cannot be evaluated independently of the response-removal procedure.

These findings are particularly relevant for modern dense monitoring systems, including urban seismic networks, distributed broadband arrays, and emerging low-cost MEMS-based deployments. In such configurations, improvements in instrumental self-noise, response stability, and environmental-noise mitigation may become as important as — or more important than — further network densification.

Several limitations nevertheless constrain the present framework. The environmental-noise model is synthetic and temporally stationary, realistic phase-picking and event-association procedures are not explicitly modeled, and three-dimensional propagation effects are neglected. Consequently, the resulting detectability fields should be interpreted as physically informed sensitivity patterns rather than operational estimates of catalogue completeness.

Despite these limitations, the framework provides a computationally reproducible and physically transparent basis for investigating the transition between geometry-controlled and instrumentation-controlled monitoring regimes. The methodology further establishes a direct conceptual bridge between instrumental seismology and

https://doi.org/10.5194/egusphere-2026-2672
Preprint. Discussion started: 23 June 2026

probabilistic seismic-network performance analysis by explicitly incorporating response-corrected instrumental self-noise into network-scale detectability metrics.

By explicitly propagating response-corrected instrumental self-noise into network-scale detectability metrics, the present study reframes seismic-network performance as an emergent multiscale property linking instrument physics, environmental noise, and spatial network organization within a unified probabilistic framework.

Future developments should incorporate empirical PSD archives, instrument-specific self-noise measurements, realistic propagation simulations, and machine-learning-based detection frameworks. Such extensions would allow the present methodology to evolve toward fully operational detectability forecasting systems capable of supporting next-generation seismic-network optimization and performance assessment.

Competing interests:

The authors declare that they have no conflict of interest.

8. References

Allen, R. V.: Automatic earthquake recognition and timing from single traces, Bull. Seismol. Soc. Am., 68, 1521–1532, https://doi.org/10.1785/BSSA0680051521, 1978.

Anthony, R. E., Ringler, A. T., Wilson, D. C., and Wolin, E.: Do low-cost seismographs perform well enough for your network? An overview of laboratory tests and field observations of the OSOP Raspberry Shake 4D, Seismol. Res. Lett., 90, 219–228, https://doi.org/10.1785/0220180251, 2019.

Catania, M., Figlioli, A., Vitale, G., and D'Alessandro, A.: Seismic noise characterization of broad-band stations in the Italian region using power spectral density: a frequency, spatial and statistical analysis, Geophys. J. Int., 242, ggaf168, https://doi.org/10.1093/gji/ggaf168, 2025.

https://doi.org/10.5194/egusphere-2026-2672
Preprint. Discussion started: 23 June 2026

D'Alessandro, A. and D'Anna, G.: Suitability of low-cost three-axis MEMS accelerometers in strong-motion seismology: tests on the LIS331DLH (iPhone) accelerometer, Bull. Seismol. Soc. Am., 103, 2906–2913, https://doi.org/10.1785/0120120287, 2013.

D'Alessandro, A. and Ruppert, N.: Evaluation of location performance and magnitude of completeness of Alaska Regional Seismic Network by SNES method, Bull. Seismol. Soc. Am., 102, 2098–2115, https://doi.org/10.1785/0120110199, 2012.

D'Alessandro, A. and Stickney, M.: Montana Seismic Network Performance: an evaluation through the SNES method, Bull. Seismol. Soc. Am., 102, 73–87, https://doi.org/10.1785/0120100234, 2012.

D'Alessandro, A., D'Anna, G., Luzio, D., and Mangano, G.: Seismic Network Evaluation through Simulation: An Application to the Italian National Seismic Network, Bull. Seismol. Soc. Am., 101, 1213–1232, https://doi.org/10.1785/0120100066, 2011.

D'Alessandro, A., Gervasi, A., and Guerra, I.: Evolution and strengthening of the Calabrian Regional Seismic Network, Adv. Geosci., 36, 11–16, https://doi.org/10.5194/adgeo-36-11-2013, 2013.

D'Alessandro, A., Luzio, D., and D'Anna, G.: Urban MEMS based seismic network for post-earthquakes rapid disaster assessment, Adv. Geosci., 40, 1–9, https://doi.org/10.5194/adgeo-40-1-2014, 2014.

D'Alessandro, A., Vitale, G., Scudero, S., D'Anna, R., Costanza, A., Fagiolini, A., and Greco, L.: Characterization of MEMS accelerometer self-noise by means of PSD and Allan variance analysis, in: 2017 IEEE 7th International Workshop on Advances in Sensors and Interfaces (IWASI), 159–164, https://doi.org/10.1109/IWASI.2017.7974238, 2017.

https://doi.org/10.5194/egusphere-2026-2672
Preprint. Discussion started: 23 June 2026

D'Alessandro, A., Greco, L., Scudero, S., and Lauciani, V.: Spectral characterization and spatiotemporal variability of the background seismic noise in Italy, Earth Space Sci., 8, e2020EA001579, https://doi.org/10.1029/2020EA001579, 2021.

EIDA Consortium: European Integrated Data Archive (EIDA), available at: https://www.orfeus-eu.org/data/eida/ (last access: 9 May 2026), 2023.

Gerner, A. and Bokelmann, G.: Instrument self-noise and sensor misalignment, Adv. Geosci., 36, 17–23, https://doi.org/10.5194/adgeo-36-17-2013, 2013.

IRIS DMC: IRIS Data Services, available at: https://ds.iris.edu/ds/nodes/dmc/ (last access: 9 May 2026), 2014.

McNamara, D. E. and Buland, R. P.: Ambient noise levels in the continental United States, Bull. Seismol. Soc. Am., 94, 1517–1527, https://doi.org/10.1785/012003001, 2004.

Peterson, J.: Observations and modeling of seismic background noise, U.S. Geol. Surv. Open-File Rep. 93-322, 95 pp., https://doi.org/10.3133/ofr93322, 1993.

Ringdal, F.: On the estimation of seismic detection thresholds, Bull. Seismol. Soc. Am., 65, 1631–1642, https://doi.org/10.1785/BSSA0650061631, 1975.

Ringdal, F. and Kværna, T.: A multi-channel processing approach to real time network detection, phase association, and threshold monitoring, Bull. Seismol. Soc. Am., 79, 1927–1940, https://doi.org/10.1785/BSSA0790061927, 1989.

Ringler, A. and Hutt, C. R.: Self-noise models of seismic instruments, Seismol. Res. Lett., 81, 972–983, https://doi.org/10.1785/gssrl.81.6.972, 2010.

https://doi.org/10.5194/egusphere-2026-2672
Preprint. Discussion started: 23 June 2026

Ruzza, G., Cogliano, R., D'Ambrosio, C., Falco, L., Cardinale, V., Minichiello, F., Memmolo, A., Castagnozzi, A., De Luca, G., and Vicari, A.: SEISMONOISY: A quasi-real-time seismic noise network monitoring system, Sensors, 24, 3474, https://doi.org/10.3390/s24113474, 2024.

Scherbaum, F.: Of Poles and Zeros: Fundamentals of Digital Seismology, 2nd edn., Springer, Dordrecht, https://doi.org/10.1007/978-1-4020-6861-4, 2001.

Scudero, S., Vitale, G., D'Alessandro, A., D'Anna, R., Costanza, A., Fagiolini, A., and Greco, L.: Urban seismic networks: a worldwide review, Appl. Sci., 13, 13165, https://doi.org/10.3390/app132413165, 2023.

Sleeman, R., van Wettum, A., and Trampert, J.: Three-channel correlation analysis: a new technique to measure instrumental noise of digitizers and seismic sensors, Bull. Seismol. Soc. Am., 96, 258–271, https://doi.org/10.1785/0120050032, 2006.

Trnkoczy, A.: Understanding and parameter setting of STA/LTA trigger algorithm, in: New Manual of Seismological Observatory Practice 2 (NMSOP-2), edited by: Bormann, P., Deutsches GeoForschungsZentrum GFZ, Potsdam, 1–20, https://doi.org/10.2312/GFZ.NMSOP-2_IS_8.1, 2012.

Vitale, G., D'Alessandro, A., Di Benedetto, A., Figlioli, A., Costanzo, A., Speciale, S., Piattoni, Q., and Cipriani, L.: Urban seismic network based on MEMS sensors: the experience of the seismic observatory in Camerino (Marche, Italy), Sensors, 22, 4335, https://doi.org/10.3390/s22124335, 2022.

Wang, K., Li, W., Zhang, L., Yang, D., Wang, X., and Zhao, J.: Research on self-noise characteristics of nine types of seismometers obtained by PDF representation using continuous seismic data from the Malingshan Seismic Station, China, Sensors, 23, 110, https://doi.org/10.3390/s23010110, 2023.

https://doi.org/10.5194/egusphere-2026-2672
Preprint. Discussion started: 23 June 2026

Wielandt, E.: Seismic sensors and their calibration, in: International Handbook of Earthquake and Engineering Seismology, Part A, edited by: Lee, W. H. K., Kanamori, H., Jennings, P. C., and Kisslinger, C., Int. Geophys. Ser., 81A, Academic Press, San Diego, 283–304, https://doi.org/10.1016/S0074-6142(02)80298-9, 2002.

Withers, M., Aster, R., Young, C., and Chael, E.: High-frequency analysis of seismic background noise as a function of wind speed and shallow depth, Bull. Seismol. Soc. Am., 86, 1507–1515, https://doi.org/10.1785/BSSA0860051507, 1996.

Woessner, J. and Wiemer, S.: Assessing the quality of earthquake catalogues: estimating the magnitude of completeness and its uncertainty, Bull. Seismol. Soc. Am., 95, 684–698, https://doi.org/10.1785/0120040007, 2005.

https://doi.org/10.5194/egusphere-2026-2672
Preprint. Discussion started: 23 June 2026

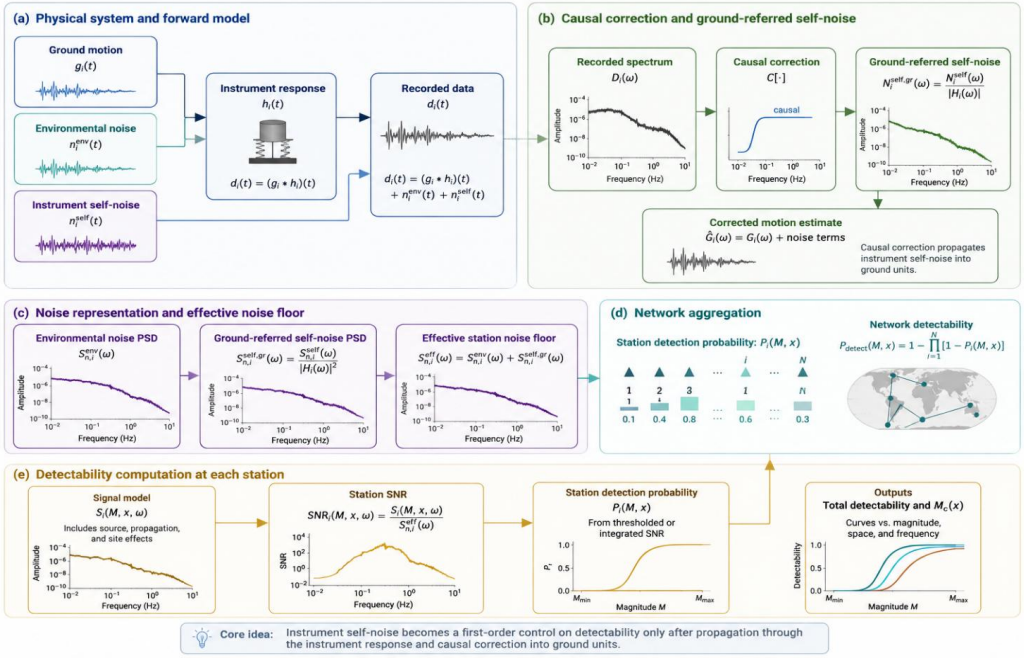

Figure 1. *Conceptual framework linking causal instrument correction to network-scale seismic detectability. Panel (a) summarizes the observational model at station i, where recorded data result from the convolution of ground motion with the instrumental response in the presence of environmental and instrumental noise contributions. Panel (b) illustrates causal response correction and the propagation of instrumental self-noise into ground-referred units after inverse filtering. Panel (c) defines the effective station noise floor resulting from the combined contribution of environmental noise and propagated self-noise. Panel (d) shows the station-level detectability concept based on signal-to-noise ratio and probabilistic detection. Panel (e) extends the formulation to the network scale through probabilistic aggregation of station detections into spatial detectability and completeness-magnitude fields. The figure summarizes the physical and computational chain linking instrument-response physics to large-scale seismic-network performance.*

https://doi.org/10.5194/egusphere-2026-2672
Preprint. Discussion started: 23 June 2026

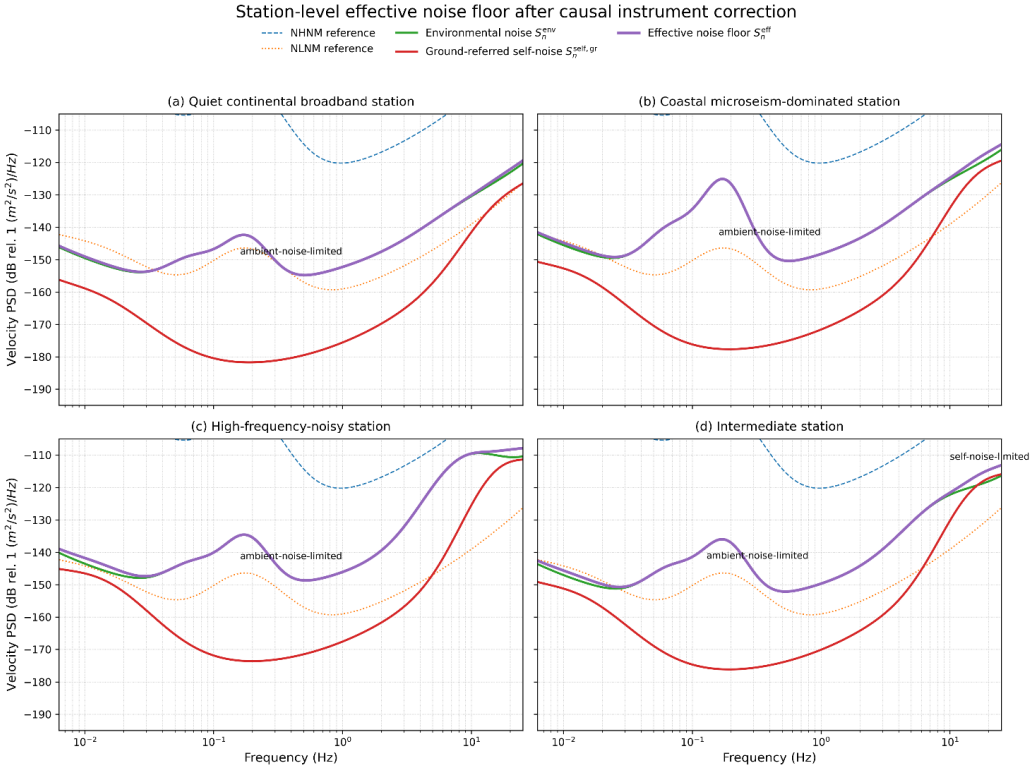

Figure 2. *Station-level effective noise floor after causal instrument correction. Panels (a–d) show representative power spectral density (PSD) models for four broadband seismic stations characterized by different environmental conditions: (a) quiet continental site, (b) coastal microseism-dominated site, (c) high-frequency noisy site, and (d) intermediate conditions. Environmental noise spectra (green) and ground-referred instrumental self-noise (red), obtained after causal response correction, are combined into the effective station noise floor (purple). Dashed and dotted curves denote the NHNM and NLNM reference models of Peterson (1993). The results illustrate how instrumental self-noise becomes frequency dependent after response correction and may contribute significantly to the effective station noise floor under low-noise conditions or near the limits of the instrumental passband. Although environmental noise dominates most frequency bands, propagated self-noise establishes a lower bound on achievable signal-to-noise ratio and therefore on seismic detectability.*

https://doi.org/10.5194/egusphere-2026-2672
Preprint. Discussion started: 23 June 2026

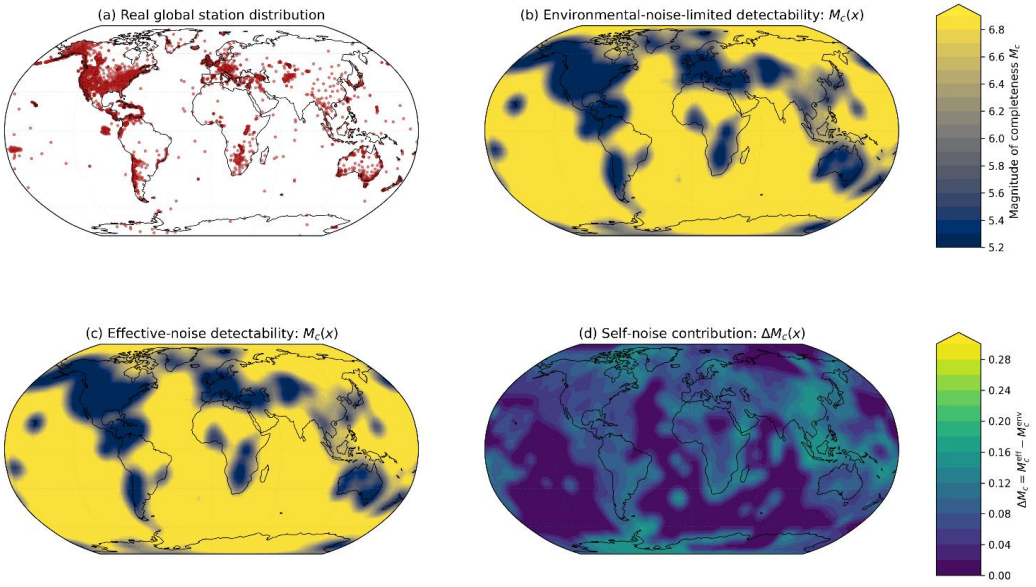

Figure 3. *Global detectability and completeness under environmental and effective station noise. Panel (a) shows the spatial distribution of broadband seismic stations derived from open FDSN Station services (EarthScope and EIDA federator), highlighting the strong heterogeneity of the present-day global monitoring infrastructure. Panel (b) presents the spatial distribution of completeness magnitude* $M_c(x)$ *computed using environmental noise only within the probabilistic detectability framework described in the text. Low* M_c *values coincide with densely instrumented regions, whereas sparsely monitored areas exhibit substantially reduced detectability. Panel (c) shows the corresponding completeness field after inclusion of propagated instrumental self-noise within the effective station noise model. The resulting detectability is systematically degraded, leading to higher completeness magnitude values. Panel (d) illustrates the spatial increment in completeness magnitude associated with instrumental self-noise. Although generally moderate, the effect is spatially heterogeneous and becomes more pronounced in regions characterized by sparse geometry and elevated effective station noise. Spatial fields are mildly smoothed for visualization purposes only and do not affect the underlying detectability calculations.*

https://doi.org/10.5194/egusphere-2026-2672
Preprint. Discussion started: 23 June 2026

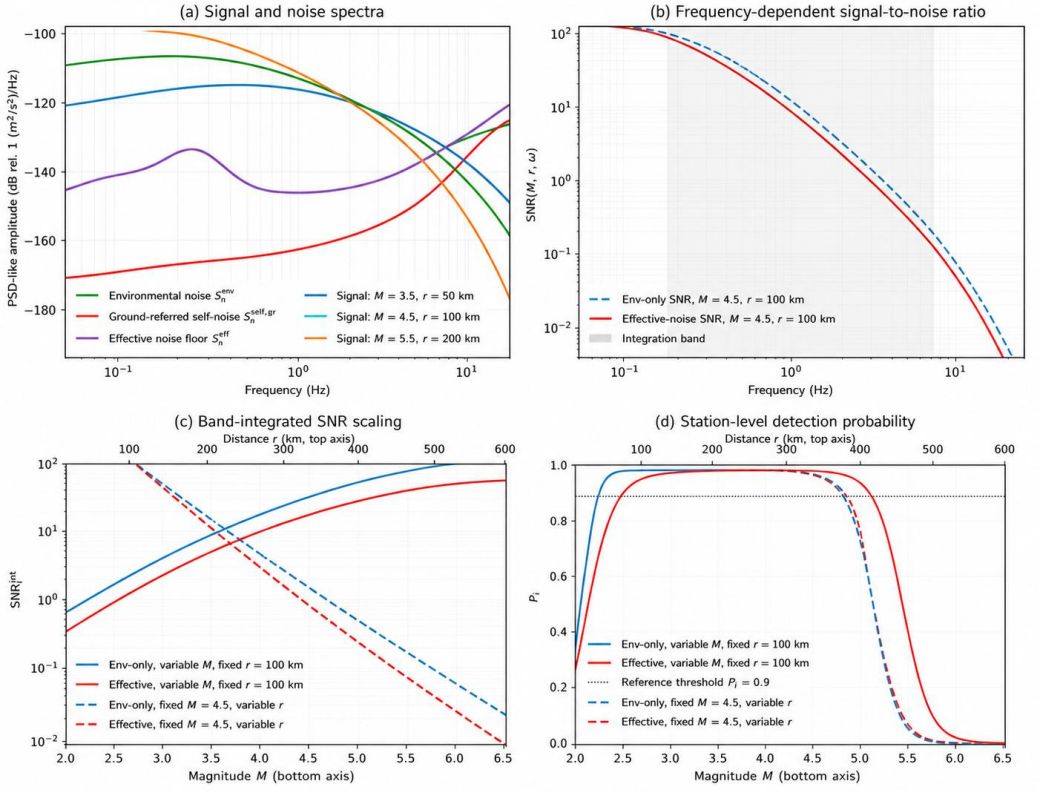

Figure 4. *Frequency-dependent propagation of effective station noise into signal-to-noise ratio and station-level detectability. Panel (a) shows representative environmental-noise spectra, propagated instrumental self-noise, effective station noise floor, and theoretical earthquake signal spectra for different magnitude–distance combinations. The effective station noise floor results from the combination of environmental and ground-referred instrumental self-noise after causal response correction. Panel (b) illustrates the frequency-dependent signal-to-noise ratio obtained using environmental noise only (blue) and the full effective noise model (red) for a representative event scenario. The shaded region indicates the integration band adopted for detectability calculations. Panel (c) shows the dependence of integrated signal-to-noise ratio on earthquake magnitude (solid curves) and epicentral distance (dashed curves), comparing environmental-noise-only and effective-noise conditions. Panel (d) presents the corresponding probabilistic station detection curves. The results demonstrate that propagated instrumental self-noise systematically reduces detectability, particularly near the lower signal-to-noise threshold and at larger source–receiver distances.*

https://doi.org/10.5194/egusphere-2026-2672
Preprint. Discussion started: 23 June 2026

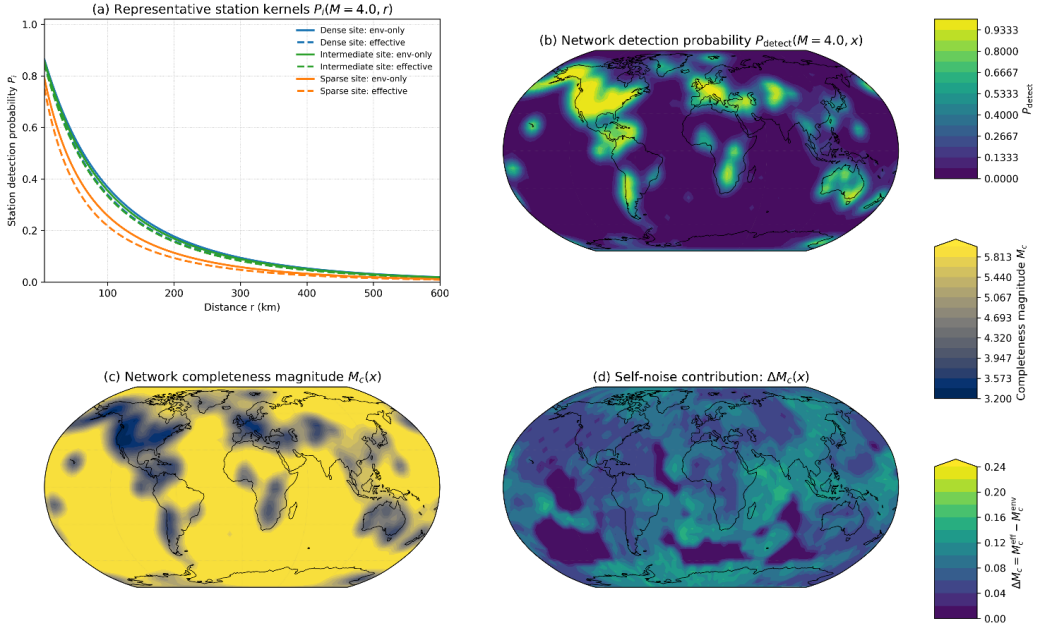

874

875 **Figure 5.** *From station-level detectability kernels to network-scale completeness structure.*
876 *Panel (a) shows representative station-detection kernels for dense, intermediate, and sparse monitoring*
877 *configurations, comparing environmental-noise-only and effective-noise conditions. Detection probability*
878 *decreases with increasing source–receiver distance and is systematically reduced when propagated*
879 *instrumental self-noise is included. Panel (b) presents the resulting global network detection probability field*
880 *for a representative earthquake magnitude. High detectability is concentrated in densely instrumented*
881 *continental regions, whereas oceanic and poorly monitored areas exhibit substantially lower detection*
882 *capability. Panel (c) shows the corresponding spatial completeness-magnitude field* $M_c(x)$*, highlighting the*
883 *strong geographical heterogeneity of global seismic-network performance. Panel (d) illustrates the increase*
884 *in completeness magnitude associated with propagated instrumental self-noise. Although generally moderate,*
885 *this degradation becomes spatially coherent and regionally significant when integrated over large-scale*
886 *network configurations.*

https://doi.org/10.5194/egusphere-2026-2672
Preprint. Discussion started: 23 June 2026

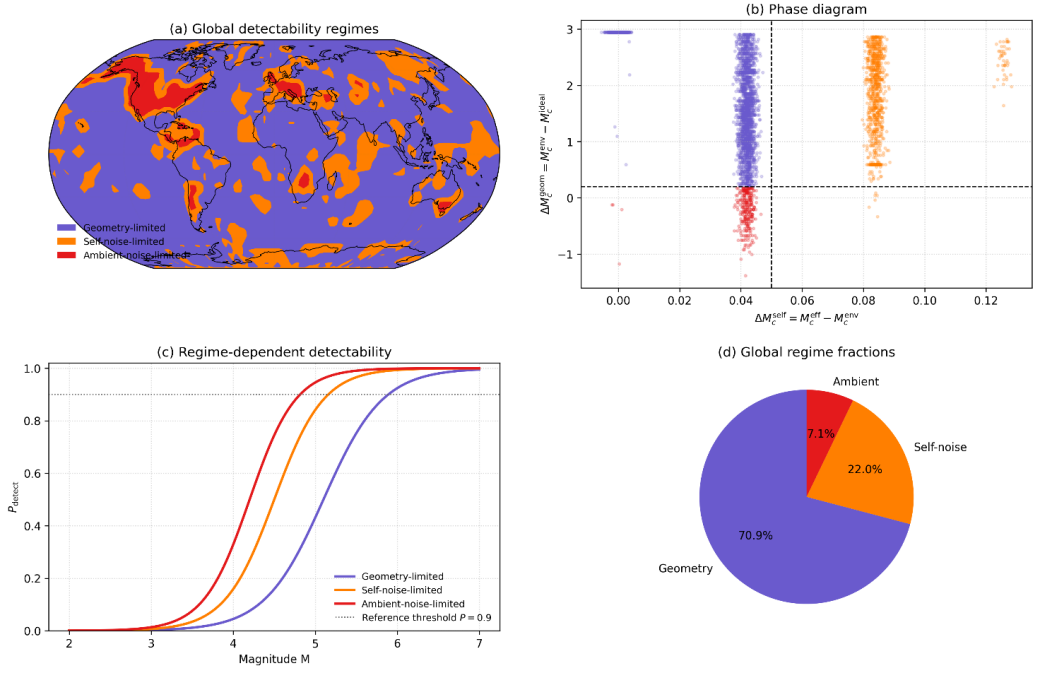

Figure 6. *Global classification of detectability regimes. Panel (a) shows the spatial distribution of the dominant detectability regimes derived from the relative contributions of network geometry, environmental noise, and propagated instrumental self-noise. Three principal regimes are identified: geometry-limited, self-noise-limited, and ambient-noise-limited. Panel (b) presents the corresponding phase diagram in the space defined by effective self-noise contribution and geometry-related detectability degradation. The dashed lines denote reference transition thresholds separating the dominant-control domains. Panel (c) illustrates representative detectability curves for the three regimes, demonstrating the systematic shift in completeness magnitude associated with changing dominant controls. Panel (d) summarizes the global fractional occupancy of each regime. The results show that sparse monitoring geometries dominate most large-scale detectability limitations, whereas instrumental self-noise becomes increasingly important in dense and low-noise monitoring environments.*

https://doi.org/10.5194/egusphere-2026-2672
Preprint. Discussion started: 23 June 2026

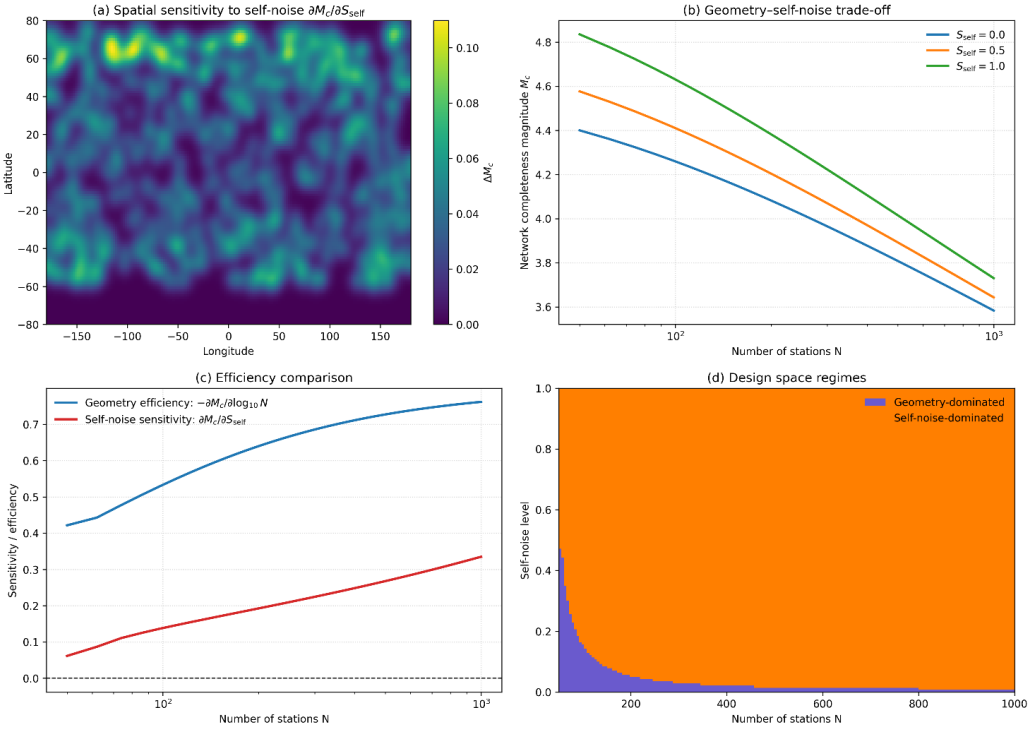

Figure 7. *Sensitivity analysis of geometry-driven and instrumentation-driven detectability controls. Panel (a) shows the spatial sensitivity of completeness magnitude to propagated instrumental self-noise, illustrating the heterogeneous geographical response of detectability to sensor-quality degradation. Panel (b) presents the trade-off between network densification and instrumental self-noise reduction for different effective self-noise levels. Increasing station density systematically improves detectability, although the relative gain decreases as networks become progressively denser. Panel (c) compares the relative efficiency of geometry improvement and self-noise reduction as functions of network size. Geometry-driven gains dominate sparse configurations, whereas instrumentation-driven improvements become progressively more relevant in dense networks. Panel (d) summarizes the resulting regime-aware design space, separating geometry-dominated and self-noise-dominated optimization domains. The figure illustrates the transition from sparse geometry-controlled systems toward dense monitoring configurations in which instrumental self-noise becomes an increasingly important detectability constraint.*

https://doi.org/10.5194/egusphere-2026-2672
Preprint. Discussion started: 23 June 2026

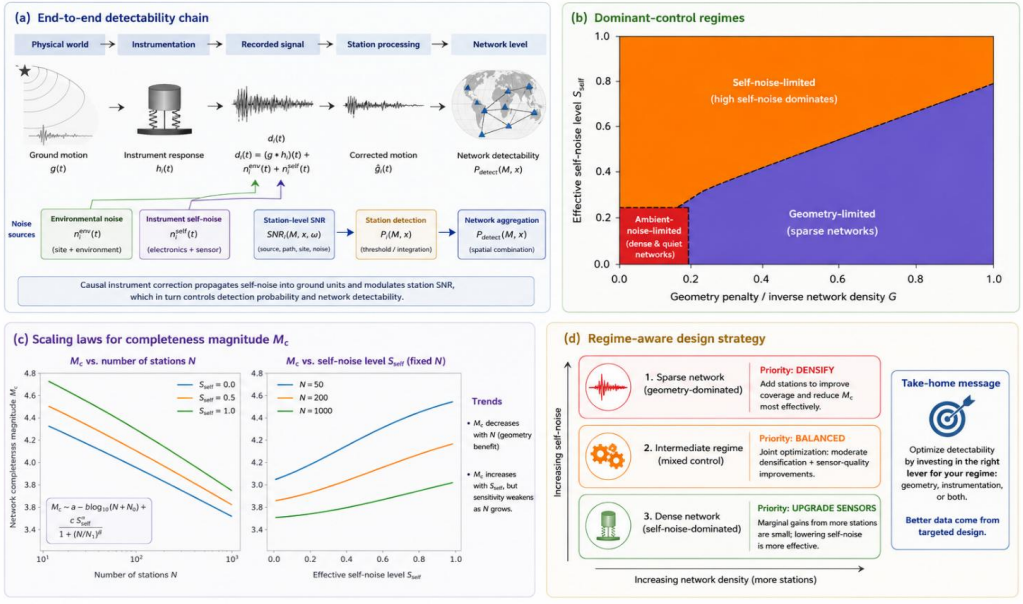

Figure 8. *Unified conceptual synthesis of the proposed detectability framework. Panel (a) summarizes the end-to-end physical and computational chain linking ground motion, instrumental response, environmental noise, propagated instrumental self-noise, station-level signal-to-noise ratio, probabilistic station detection, and network-scale detectability. Panel (b) illustrates the dominant detectability-control regimes in the space defined by geometry-related degradation and effective self-noise level, highlighting the transition from ambient-noise-limited to geometry-limited and self-noise-limited monitoring conditions. Panel (c) shows representative scaling laws for completeness magnitude as functions of network density and propagated self-noise. Panel (d) summarizes the corresponding regime-aware optimization strategy for seismic-network design. Sparse networks primarily benefit from densification, whereas dense and low-noise monitoring systems increasingly benefit from reductions in instrumental self-noise. Together, the panels synthesize the central conceptual result of the study: seismic-network detectability emerges from the coupled multiscale interaction between instrument physics, environmental noise, and network geometry.*